Arm movements induced by noninvasive optogenetic stimulation of the motor cortex in the common marmoset

Teppei Ebina[a], Keitaro Obara[a], Akiya Watakabe[b], Yoshito Masamizu[a,c,d], Shin-Ichiro Terada[a], Ryota Matoba[a], Masafumi Takaji[b], Nobuhiko Hatanaka[e], Atsushi Nambu[e], Hiroaki Mizukami[f], Tetsuo Yamamori[b], and Masanori Matsuzaki[a,c,g,1]

[a]Department of Physiology, Graduate School of Medicine, University of Tokyo, 113-0033 Tokyo, Japan; [b]Laboratory for Molecular Analysis of Higher Brain Function, RIKEN Center for Brain Science, 351-0198 Saitama, Japan; [c]Brain Functional Dynamics Collaboration Laboratory, RIKEN Center for Brain Science, 351-0198 Saitama, Japan; [d]Japan Science and Technology Agency, Precursory Research for Embryonic Science and Technology, 332-0012 Saitama, Japan; [e]Division of System Neurophysiology, National Institute for Physiological Sciences, School of Life Science, The Graduate University for Advanced Studies (SOKENDAI), 444-8585 Aichi, Japan; [f]Division of Genetic Therapeutics, Center for Molecular Medicine, Jichi Medical University, 329-0498 Tochigi, Japan; and [g]International Research Center for Neurointelligence, The University of Tokyo Institutes for Advanced Study, 113-0033 Tokyo, Japan

Edited by Peter L. Strick, University of Pittsburgh, Pittsburgh, PA, and approved October 4, 2019 (received for review February 28, 2019)

Optogenetics is now a fundamental tool for investigating the relationship between neuronal activity and behavior. However, its application to the investigation of motor control systems in nonhuman primates is rather limited, because optogenetic stimulation of cortical neurons in nonhuman primates has failed to induce or modulate any hand/arm movements. Here, we used a tetracycline-inducible gene expression system carrying CaMKII promoter and the gene encoding a Channelrhodopsin-2 variant with fast kinetics in the common marmoset, a small New World monkey. In an awake state, forelimb movements could be induced when Channelrhodopsin-2–expressing neurons in the motor cortex were illuminated by blue laser light with a spot diameter of 1 mm or 2 mm through a cranial window without cortical invasion. Forelimb muscles responded 10 ms to 50 ms after photostimulation onset. Long-duration (500 ms) photostimulation induced discrete forelimb movements that could be markerlessly tracked with charge-coupled device cameras and a deep learning algorithm. Long-duration photostimulation mapping revealed that the primary motor cortex is divided into multiple domains that can induce hand and elbow movements in different directions. During performance of a forelimb movement task, movement trajectories were modulated by weak photostimulation, which did not induce visible forelimb movements at rest, around the onset of task-relevant movement. The modulation was biased toward the movement direction induced by the strong photostimulation. Combined with calcium imaging, all-optical interrogation of motor circuits should be possible in behaving marmosets.

optogenetics | Channelrhodopsin-2 | common marmosets | motor cortex | forelimb

Optogenetics has been applied to manipulate the neuronal activity related to a variety of brain functions in nonhuman primates (1–6) and rodents. With regard to the motor control system of nonhuman primates, saccadic eye movements were modulated by optogenetic activation and/or inactivation of cerebral cortical neurons (7–11). However, optogenetic stimulation failed to induce or modulate any limb movements in nonhuman primates, even though motor cortical neurons were activated (2, 4, 12). This is in contrast to mice, in which Channelrhodopsin-2 (ChR2) stimulation of layer 5 neurons in multiple subregions of the motor cortex successfully induced different types of complex forelimb movements (13, 14). This may be because the number of photoactivated neurons in the nonhuman primate did not reach a level sufficient to elicit hand/arm movements, and/or because the activation patterns of neurons and/or the types of activated neurons differ between optogenetic and electrical stimulation (2, 15, 16).

In this study, we used the common marmoset (*Callithrix jacchus*) to overcome these possible problems, as this New World monkey has a smaller motor cortex than macaque and squirrel monkeys. We therefore expected it to be easier to photostimulate a relatively larger proportion of the motor cortical neurons dominating the hand/arm movements. To do this, we used adeno-associated viruses (AAVs) with a tetracycline-inducible gene expression (TET-inducible) system that amplifies neuronal expression of induced genes. We previously used this system carrying the GCaMP gene to establish 2-photon calcium imaging of cortical neurons in anesthetized and behaving marmosets (17, 18). We also used a ChR2 variant (E123T/T159C) with fast kinetics (19) that was able to follow each high-frequency photostimulation, as is commonly used in electrical stimulation (100 Hz to 350 Hz; ref. 15). Furthermore, we used a cranial window to permit stimulation of a larger area (diameter of 1 mm to 2 mm) than is possible with an optical fiber inserted into the cortex.

Significance

Which brain area drives hand/arm movements after learning or brain injury? When does motor cortical activity generate appropriate hand/arm movements? To address these issues, it is necessary to manipulate motor cortical activity in a controlled manner. Optogenetic tools allow neuronal activity to be manipulated in a variety of animals, but forelimb movements in nonhuman primates have not previously been optogenetically induced or modulated. Here, we improved a method of optogenetic cortical stimulation and induced overt forelimb movements in the common marmoset, a New World monkey. Photostimulation also modulated voluntary forelimb movements, with the modulated movement trajectories depending on the stimulation site and timing. Our results open doors for noninvasive interrogation of motor circuits in behaving nonhuman primates.

Author contributions: T.E., Y.M., and M.M. designed research; T.E., K.O., A.W., and Y.M. performed research; T.E., A.W., S.-I.T., M.T., N.H., A.N., H.M., and T.Y. contributed new reagents/analytic tools; T.E., K.O., and R.M. analyzed data; and T.E. and M.M. wrote the paper.

The authors declare no competing interest.

This article is a PNAS Direct Submission.

Data deposition: The data for the photostimulation-induced movements used in Figs. 1–4 have been deposited in Figshare (https://dx.doi.org/10.6084/m9.figshare.9918887).

[1]To whom correspondence may be addressed. Email: mzakim@m.u-tokyo.ac.jp.

This article contains supporting information online at www.pnas.org/lookup/suppl/doi:10.1073/pnas.1903445116/-/DCSupplemental.

First published October 21, 2019.

Results

Hand Movement Was Induced by Photostimulation of the Motor Cortex in ChR2-Expressing Awake Marmosets. We performed intracortical electrical microstimulation (ICMS) to identify the right M1 region dominating left forelimb movement in 2 awake common marmosets (marmosets E and F; *SI Appendix*, Fig. S1*A*). Within the identified area, a mixture of 3 AAVs encoding Thy1S-tetracycline-controlled transactivator (tTA), CaMKII-Cre, and the tetracycline response element (TRE)-flex-ChR2 variant (E123T/T159C)-enhanced yellow fluorescent protein (EYFP) was injected into 6 sites (18). Then, a 4.5-mm or 5.5-mm circular glass window attached to a titanium chamber was put over the injected area (*SI Appendix*, Fig. S1 *B* and *C*). We observed obvious EYFP fluorescence around the injection sites 4 wk to 6 wk after the injection (*SI Appendix*, Fig. S1*C*). EYFP fluorescence was detected in 18.0 ± 1.9% of neurons (mean ± SD, $n = 5$ imaging areas, a total of 187 EYFP-positive neurons out of 1,044 propidium iodide-positive neurons) in the cortical tissue 484 d after the virus injection, and 8.7 ± 3.1% of the EYFP-positive neurons were parvalbumin-positive ($n = 3$ imaging areas, a total of 8 parvalbumin-positive neurons out of 83 EYFP-positive neurons; *SI Appendix*, Fig. S1 *D–F*). We also injected a mixture of AAVs encoding Thy1S-tTA, CaMKII-Cre, and TRE-flex-Clover (20) into the cortex of another marmoset to investigate the ratios of excitatory and inhibitory neurons to GFP (Clover)-positive neurons by immuno-in situ hybridization for VGLUT1 (excitatory) and GAD67 (inhibitory) genes. We found that 1 mo after injection, 89.2 ± 7.9% of Clover-expressing neurons were VGLUT1-positive ($n = 6$ imaging areas, 157 out of 174), while 11.0 ± 6.6% were GAD67-positive ($n = 8$ imaging areas, 29 out of 253; *SI Appendix*, Fig. S1 *G–I*). This result is consistent with the histology of the ChR2-injected marmosets. Our results suggest that, in our expression system, ∼90% of the transgene-positive neurons are excitatory and 10% are inhibitory.

Before the photostimulation sessions started, the animals were habituated to the head-fixed and loosely trunk-restrained condition, and were trained to perform forelimb movement tasks (ref. 17 and *SI Appendix*, Fig. S2). We used an optical fiber to illuminate blue laser light onto the ChR2-expressing M1 through the cranial window of the awake head-fixed marmosets (Fig. 1 *A* and *B*). The spot diameter was set to 2 mm (Fig. 1*A* and *SI Appendix*, Fig. S1 *A* and *C*). Five pulses of 5-ms-duration blue laser light (450 nm, 38 mW) were illuminated at 100 Hz. Movements of the left forelimb were captured by 2 high-speed charge-coupled device (CCD) cameras recording at 100 Hz. The position of the left hand was successfully tracked with the deep learning-based software DeepLabCut (ref. 21 and Fig. 1 *C–F*), without any optical markers being attached to the body part, thereby allowing free movement of the hand. We found that the photostimulation induced a small but stable hand movement (Fig. 1 *C–E*). We also photostimulated the same area with the laser running at decreased power levels (21.1 and 3.9 mW; Fig. 1 *F* and *G*). In both marmosets, the strong (38.0 mW) and midstrength (21.1 mW) photostimulation induced significant hand movements compared with the non-photostimulation control condition, while the weak (3.9 mW) stimulation did not induce such movements (Fig. 1 *F–H*). Similar hand movement was induced even when the diameter of the illumination spot was reduced to 1 mm (*SI Appendix*, Fig. S3). When the strong and midstrength stimuli were used, hand movement was detected in all trials, and the latency from the photostimulation onset to the movement onset was ∼60 ms (Fig. 1*I*). These latencies were similar to those induced by 500-ms ICMS in macaque M1 (22). These results clearly indicate that the repetitive 50-ms photostimulation of ChR2-expressing M1 induced a small but significant hand movement in awake marmosets.

Photostimulation of M1 Induced Short-Latency Arm Muscle Activity. We also observed that the surface electromyogram (sEMG) recordings of the biceps, triceps, extensor, and flexor muscles responded to repetitive 50-ms photostimulation (5 pulses of 5-ms duration at 100 Hz and 38.0 mW). *SI Appendix*, Fig. S4*A* shows the raw sEMG of the biceps muscle evoked by photostimulation. In marmoset E, the biceps, triceps, and extensor muscles showed significant changes in the averaged and rectified sEMGs from 10 ms to 40 ms after photostimulation onset. In marmoset F, the sEMGs of the biceps and flexor muscles significantly changed from 20 ms to 50 ms after the onset (*SI Appendix*, Fig. S4*B*). Thus, the photostimulation of ChR2-expressing M1 in the awake marmoset evoked muscle activity with a delay of ∼20 ms. This latency is

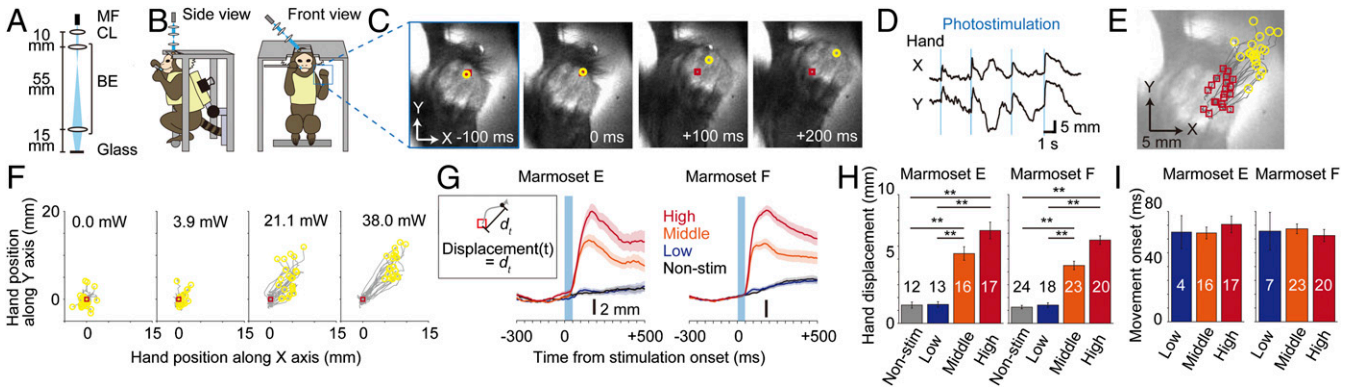

Fig. 1. Photostimulation of M1 in ChR2-expressing marmoset induces hand movements. (*A*) Scheme of the light path for the photostimulation. Multimode optical fiber (MF), collimating lens (CL), and lenses of the beam expander (BE) are separated by the distances indicated in the panel. (*B*) Scheme of the marmoset in the apparatus. The light was introduced perpendicular to the cranial window. The square outlined in blue represents the camera recording area shown in *C*. (*C*) Hand images at 4 time points in a representative photostimulation trial. Yellow circles indicate the hand position (the root of the middle finger) at the 4 time points from the stimulation onset tracked by DeepLabCut. Red squares indicate the averaged hand position across −300 ms to 0 ms from stimulation onset (defined as original position) and are located at the same position across the 4 images. (*D*) Example X- and Y-trajectories of the hand position across 4 photostimulation trials. (*E*) Superimposed original (red squares) and end (yellow circles) positions and hand trajectories (gray) in 20 photostimulation trials. (*F*) Hand trajectories relative to their original positions at the different stimulation strengths. (*G*) Displacement of the hand position. Red, orange, and blue lines represent the trial-averaged displacements induced by high, middle, and low-strength photostimulation, respectively. Black lines are the trial-averaged displacements in the nonstimulation trials. Shaded areas represent the SEM. (*H*) The amplitudes of hand displacements at the different stimulation strengths. Bars represent mean ± SEM $^{**}P < 0.01$. (*I*) Hand movement onsets at the different stimulation strengths. Only trials with displacements exceeding the mean + 5.0 SD of those in the prestimulation period were analyzed. *P* values in the Kruskal–Wallis test were >0.05.

within the range of the values measured for muscle activity evoked by M1 ICMS in anesthetized squirrel monkey (15.5 ms to 36.6 ms; ref. 23), thereby suggesting that photostimulation of M1 can directly evoke arm muscle responses.

Long-Duration Photostimulation of M1 Induced Discrete Forelimb Movement. Next, we increased the duration of repetitive photostimulation to 500 ms, as has also been used in ICMS experiments (22, 24), and examined the trajectories of the induced movements. Repetitive 500-ms photostimulation (50 pulses of 5-ms duration at 100 Hz and 38.0 mW) induced large and smooth continuous movements. Approximately 60 ms after the stimulation onset, left hand movements started with rotation and/or movement of the left elbow (Fig. 2 *A*–*C* and *SI Appendix*, Fig. S5 *A* and *C*). In both marmosets, the hand trajectories during the first 200 ms mostly overlapped with those induced by the 50-ms stimulation (Fig. 2 *B* and *C*). The hand trajectories in both marmosets (Fig. 2 *B* and *C*) and the elbow trajectories in marmoset F (Fig. 2*C* and *SI Appendix*, Fig. S5*C*) were stable across trials. In the trajectories with a displacement of >20 mm, the SDs of the angle of the direction from the original to end points were only 3.1° to 8.4° (Fig. 2 *D*, *Top*, and *E* and *SI Appendix*, Fig. S5*D*). The distance between the original and end hand points during the 500-ms stimulation depended on the stimulation strength, in a similar manner to the distances during the 50-ms stimulation (Fig. 2*F* and *SI Appendix*, Fig. S5*E*). With high or midstrength laser power, the hand displacement either continually increased during the 500-ms photostimulation (marmoset E) or reached a plateau before the end of the photostimulation (marmoset F). In both marmosets, the movements stopped within 200 ms after the end of the photostimulation, and their hands returned to the original position in ∼500 ms to 1,000 ms. These stable forelimb movements with clear end points were similar to those induced by 500-ms photostimulation of the mouse M1, in which ChR2 is strongly expressed in pyramidal neurons (14). These results indicate that the forelimb movement induced by the 500-ms stimulation at 100 Hz was continuous from the start point to the end point (i.e., discrete), rather than rhythmic (14, 25).

When the stimulation frequency was reduced to 10 Hz (5 pulses of 5-ms duration at 10 Hz and 38.0 mW), the movement speed reduced, and the distance between the original and end points was shorter. However, the hand displacement accumulated across the photostimulations during the entire 500-ms stimulation period, and then decreased gradually after the end of the photostimulation (Fig. 2*F* and *SI Appendix*, Fig. S5*E*). Thus, low-frequency repetitive photostimulation with a sufficiently high laser power can also induce significant forelimb movements.

In the marmoset cortex, a TET-inducible system can maintain gene expression for more than 3 mo (17, 18). Therefore, we tested the duration for which the photostimulation could stably induce hand movements (*SI Appendix*, Fig. S6). The first session of the 500-ms photostimulation experiment was performed on postinjection day 183 in marmoset E and postinjection day 58 in marmoset F. In marmoset E, the movement direction was stable until postinjection day 441 (*SI Appendix*, Fig. S6 *A* and *C*). By contrast, in marmoset F, the direction changed over postinjection days 58 to 316, although the direction was similar across near days (*SI Appendix*, Fig. S6 *B* and *D*). When the experiments started, marmoset F was younger than marmoset E, and the postinjection day on which the experiments commenced was sooner in marmoset F. Thus, the difference in the direction stability might be due to changes in the gene expression level, and/or motor cortical organization during the experimental period, being larger in marmoset F than in marmoset E. The gradual decrease in the movement displacement in both marmosets might be caused by a decrease in the gene expression level. We concluded that the photostimulation induced significant hand movements for at least 259 d, and that the induced movement direction remained similar for at least 1 wk.

Motor Mapping by Photostimulation. We mapped the left hand movement within ∼4 × 4 mm areas and presented the movement direction and displacement for each stimulation site as an arrow (*SI Appendix*, Fig. S7). In marmoset E, as the 500-ms photostimulation spot was moved from the medial to lateral axis of the cortex, the direction of the induced hand movement changed from a lateral (positive X), upward (positive Y), and forward (push, negative Z) direction to a lateral, upward, and backward (pull) direction (*SI Appendix*, Fig. S7*B*). In marmoset F, most stimulation sites exhibited the lateral, downward, and push direction (*SI Appendix*, Fig. S7*D*). Similar results were obtained with 50-ms photostimulation, although the movement directions were more varied (*SI Appendix*, Fig. S7 *B* and *D*). The sites that induced long-distance movements roughly corresponded with the sites where ICMS induced forelimb movements (*SI Appendix*, Fig. S1*A*). However, these sites were also around the virus injection sites (*SI Appendix*, Fig. S7 *A* and *C*), and, therefore, for

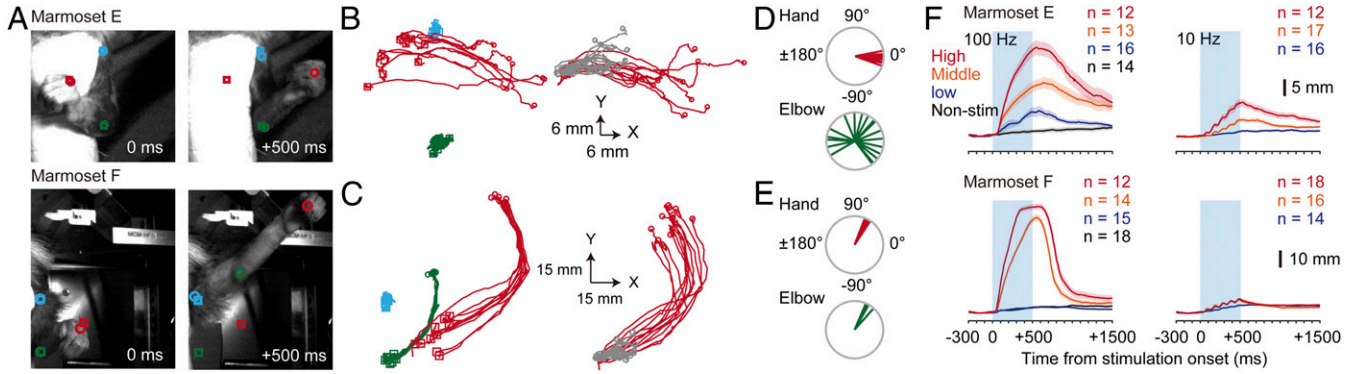

Fig. 2. Hand movements induced by long-duration photostimulation. (*A*) Examples of hand (red), elbow (green), and shoulder (cyan) positions of marmosets (*Top*) E and (*Bottom*) F at 0 and 500 ms from photostimulation onset. Squares indicate the original positions, and circles indicate the positions at the time points indicated at the bottom of the images. (*B*) (*Left*) Trajectories of the hand, elbow, and shoulder positions across −300 ms to +500 ms from stimulation onset in marmoset E ($n = 10$ trials; colors as in *A*). (*Right*) Superimposed hand trajectories induced by 50-ms (gray, $n = 17$ trials) and 500-ms photostimulation (red, $n = 12$ trials) aligned to the original positions. (*C*) The same plots as in *B*, but from marmoset F (*Left*, $n = 10$; *Right*, $n = 20$ and 12 for 50- and 500-ms stimulation, respectively). (*D*) Distribution of the direction of the hand (red) and elbow (green) movements in *B*. (*E*) The same plots as in *D*, but for marmoset F. (*F*) Displacement of the hand positions induced by the photostimulation with different stimulation strengths at 100- and 10-Hz frequencies. The session was the same across *A*–*F* for each marmoset; the sessions for the 50-ms stimulation experiments were the same sessions as in Fig. 1.

marmoset G, we conducted ICMS in a larger field, increased the virus injections sites, and placed a larger (8.2 × 4.2 mm, rectangular) cranial window than we did for marmosets E and F (Fig. 3 *A*–*C* and *SI Appendix*, Fig. S8 *A* and *B*). On the basis of the ICMS current threshold determined in movement induction and other studies (26, 27), we determined the borders between M1 and the premotor area (PM) and between M1 and the somatosensory area 3a (Fig. 3*A*). Repetitive 500-ms photostimulation to M1 and parts of PM and area 3a, including the ICMS sites that induced forelimb movements, induced hand and/or elbow movements with large movement displacement (Fig. 3 *C*–*G*). Shorter duration (50 ms) and lower laser power (8.2 mW) photostimulation in some parts of M1, PM, and area 3a induced movements with small displacements, but the direction varied (*SI Appendix*, Fig. S8 *C* and *D*). The hand and elbow movement directions gradually changed as the stimulation was moved over the putative borders between PM and M1, and between M1 and area 3a (Fig. 3 *D*–*G*). The direction and displacement of hand movement in center–lateral and upward–downward axes appeared to gradually change with different sites over the cortex (Fig. 3*D*), while the movement direction in the push–pull axis steeply changed: push, pull, and push, as the photostimulation spot was moved from the medial to lateral M1 (Fig. 3*E*). By contrast, the elbow movement direction changed once from the push to pull direction (Fig. 3*G*). Ethologically relevant movements such as climbing, hand-to mouth, and defensive movements, which accompany stereotyped movements of other parts of the body (24), were not induced at any photostimulation site. These results suggest that marmoset M1 has multiple domains responsible for discrete forelimb movements in different directions.

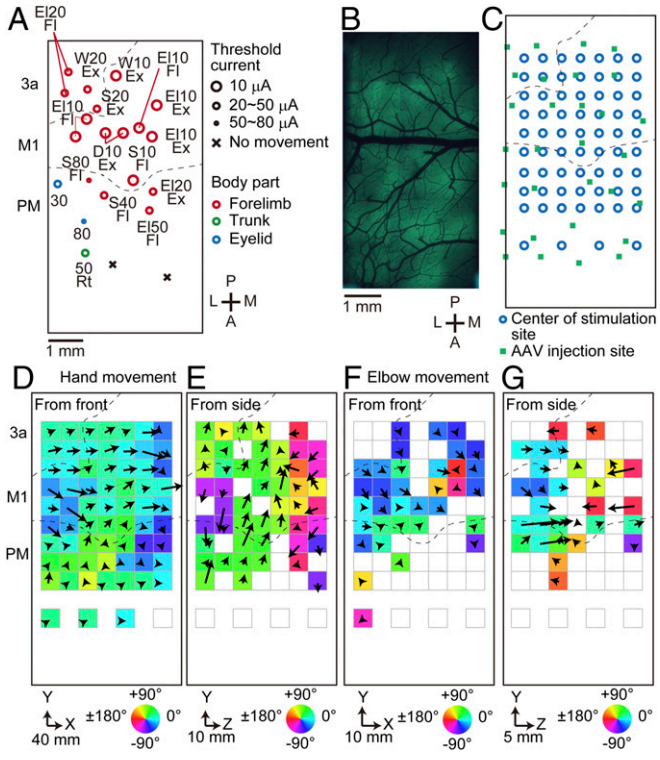

Fig. 3. Large-field motor mapping by long-duration photostimulation. (*A*) Motor mapping by ICMS in marmoset G. Dots indicate the ICMS sites that induced visible body movements. The numbers and characters next to or connected to the dots represent the threshold current required to induce the movements and the moved body parts with their movement type, respectively. D, digit; W, wrist; El, elbow; S, shoulder; Ex, extension; Fl, flexion; Rt, rotation. Crosses indicate the sites at which ICMS with ≤80-μA stimulation current induced no movement. Dotted lines indicate putative boundaries of the cortical areas. A, anterior; P, posterior; L, lateral; M, medial. (*B*) Epifluorescence image from the same mapping area as in *A* on postinjection day 45. (*C*) Distribution of photostimulation sites within the cranial window. Blue open circles indicate the center of the stimulation sites. Green squares indicate the virus injection sites. (*D*) The direction and displacement of the trial-averaged hand movement in each stimulation site are represented by the direction and length of the arrow, respectively. A color map of the movement directions is overlaid. The positive X and Y directions are lateral and upward directions, respectively. Only sites with a movement displacement of ≥4.0 mm are shown. (*E*) The same maps as in *D*, but with the left-side CCD camera. The positive Z direction is the pull direction. (*F* and *G*) The same maps as in *D* and *E*, but for the elbow movements. Only sites with a movement displacement of ≥2.0 mm are shown.

Weak Photostimulation of M1 Modulated Voluntary Forelimb Movement. When we reduced the laser power to 0.5 mW to 1.2 mW, it did not induce visible hand/arm movements at rest. Therefore, we tested whether such weak photostimulation can affect movements during voluntary motor execution, when M1 is supposed to be activated. Marmosets E and F performed a visually cued pole-pull task, in which the marmosets needed to grasp and pull a pole beyond a threshold position during a 3-s cued period to obtain a juice reward (ref. 17 and Fig. 4 *A* and *B*). We photostimulated M1 for 500 ms (50 pulses of 5-ms duration at 100 Hz and 0.5 mW to 1.2 mW) at different timings to the cue onset (Fig. 4*B*). In marmoset F, when the 500-ms photostimulation started 500 ms before the cue onset, the position of the grasped pole was slightly but significantly moved to the push direction ∼250 ms after the stimulation onset (Fig. 4 *C* and *E*). This slight movement of the pole was also observed when the photostimulation started 1,500 ms before the cue onset (Fig. 4*G*). In these cases, the reward reaching time (the time between the cue onset and the time when the pole position crossed the reward threshold) was unaffected or slightly shortened (Fig. 4 *D*, *F*, and *H*). However, photostimulation starting at the cue onset increased the reward reaching time (Fig. 4 *D*, *F*, and *H*), and photostimulation starting 500 ms after the cue onset disturbed the hand trajectory to the push direction ∼700 ms after the cue onset (Fig. 4 *C*–*H*). When the laser illumination was outside the cranial window, the pole movement and reward reaching time were unaffected (Fig. 4 *I* and *J*). In marmoset E, the photostimulation resulted in the pole being moved in the pull direction, and decreased the reward reaching time in those trials in which the photostimulation started 500 ms before the cue onset (*SI Appendix*, Fig. S9). These directions of forelimb movement induced by weak photostimulation during the task are consistent with those induced by the strong stimulation (upward push direction of elbow movement in marmoset F and upward pull direction of hand and elbow movements in marmoset E; *SI Appendix*, Fig. S5 *A* and *C*). These results indicate that the weak photostimulation of M1 modulated cortical activity in a particular period during the forelimb moving task, with a bias toward inducing similar forelimb movement to that induced by strong photostimulation.

Discussion

In this study, we demonstrated that optogenetic stimulation of M1 successfully induced forelimb movements in 3 marmosets. By contrast, earlier optogenetic studies failed to induce or modulate any hand/arm movements in nonhuman primates (2, 12). In the macaque motor cortex, optogenetic stimulation increased the firing rate of neurons, but most of the stimulation-induced activity belonged to a neural subspace that was not related to the task performance (16). The success in this study might be due to the following 2 reasons. First, to amplify ChR2 expression, we used a TET-inducible system that has been used to amplify transgene expression in rodents (28) and marmosets (17, 18), a ChR2 variant (E123T/T159C) with fast kinetics, and a relatively large light illumination spot (1 mm to 2 mm). Therefore, a larger number of neurons, whose activity might be linked to the hand movement,

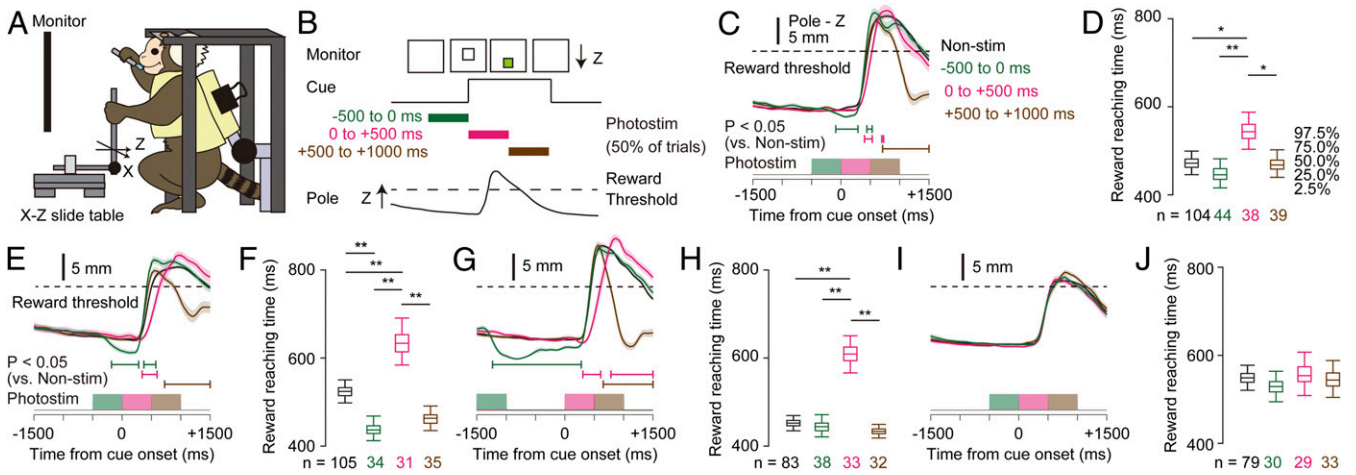

Fig. 4. Perturbation of forelimb movements by M1 photostimulation during performance of a visually cued pole-pull task. (*A*) Scheme of the task apparatus and head-fixed marmoset. (*B*) Visually cued pole-pull task and the timing of the photostimulation. The photostimulation was applied for −500 ms to 0 ms, 0 ms to 500 ms, or 500 ms to 1,000 ms from the onset of each visual cue presentation. (*C*) Traces of the Z-axial pole position during tasks with and without photostimulation in marmoset F. (*Top*) Traces of the trial-averaged Z positions of the pole. (*Middle*) Durations in which the pole positions showed statistically significant differences ($P < 0.05$) between trials with and without stimulation. (*Bottom*) Timing of the photostimulation. Black, green, magenta, and brown lines correspond to the trials without stimulation and trials with photostimulation from −500 ms to 0 ms, 0 ms to +500 ms, and +500 ms to +1,000 ms, respectively. Shaded areas in *Top* indicate the SEMs. (*D*) Reward reaching time in the 4 types of trials. Box plots represent the 95th and 50th confidence intervals of the reward reaching time in each trial type. $*P < 0.05$, $**P < 0.01$. (*E* and *F*) Traces of the Z-axial (*E*) pole position and (*F*) reward reaching time in a different session from *C*. (*G* and *H*) Traces of the Z-axial (*G*) pole position and (*H*) reward reaching time in the session in which the precue stimulation was applied at −1,500 ms from the cue onset. (*I* and *J*) Traces of the Z-axial (*I*) pole position and (*J*) reaching time in a session with the same stimulation timing as in *C*, but with the laser illumination outside of the cranial window. The *P* value in a Kruskal–Wallis test was >0.05.

would be activated than in previous studies. Second, we used marmosets, whose M1 is smaller than that of macaques. The neuronal density and light permeability may be higher (29), and, therefore, even if the same cortical volume is illuminated, a larger proportion of the motor cortical neurons that are relevant to hand/arm movements would be activated in the marmoset than in the macaque. In contrast to the macaque, the marmoset (also the squirrel monkey and mouse) makes either no or only weak direct corticomotoneuronal connections (30–32). In the marmoset and mouse, photoactivation of other types of cortical neurons may be able to effectively induce muscle responses in the forelimb (13, 14, 33). In the macaque, gene transfection into corticomotor neurons might be too inefficient to be photoactivated. It is important to investigate whether a Tet-inducible system with the current combination of AAVs and a 1- to 2-mm-diameter laser beam can be used to activate a sufficient number of corticomotor neurons and/or other types of cortical neurons to induce forelimb movements in other nonhuman primates.

Our stimulation method involving laser illumination over the cortex is much less invasive than that involving insertion of an optical fiber into the cortex. In addition to the anterior–posterior axis, if the cranial window size were to be laterally extended to ∼10 mm, the photostimulation site could cover most of the somatotopical map of the M1 and premotor cortex in the marmoset hemisphere (26), in a similar manner to covering the mouse dorsal neocortex (14). Marmosets are now being considered as a promising animal model for human psychiatric disorders, neurological disorders (34), and spinal cord injury (35), and transgenic marmoset models of a number of diseases, including spinocerebellar ataxia type 3, have been developed (36, 37). Therefore, further developments in model marmosets and stimulation techniques will allow us to clarify the long-term reorganization of the cortical body map not only during motor learning but also during rehabilitation after spinal cord injury, and will allow us to understand motor dysfunctions relevant to human psychiatric and neurological diseases.

In the present study, ethologically relevant movements (24) were not induced by 500-ms photostimulation. We think it is likely that ethologically relevant movements could be induced in the marmoset, because other New World monkeys, and even mice, show such movements (13, 14, 38). Induction of ethologically relevant movements might need the activation of a larger number of cortical neurons, especially corticospinal neurons. In addition, the stimulation parameters might need to be optimized to induce ethologically relevant movements. In our condition, the long-duration photostimulation did not induce hand movement directed toward the center of the body. This movement might be induced by activation to the more lateral (ventral) side of the motor cortex, because hand-to-central-space movement is induced by long-duration ICMS in the macaque lateral motor cortex (24). More experiments, including long-duration ICMS, are necessary to clarify the complex movement map in the marmoset.

In the visually cued pole-pull task, weak 500-ms photostimulation at any time point in respect to the cue onset caused the pole to be slightly moved in the same direction as the movement induced by the strong 500-ms stimulation. This suggests that M1 neurons are more activated by and more sensitive to photostimulation during a voluntary movement task than they are at rest. In both marmosets, the photostimulation that started 1,500 ms before the cue onset did not affect the reward reaching time, suggesting that the preceding perturbation of the M1 activity can be amended for ∼1 s before the onset of the voluntary movement. By contrast, when the photostimulation started at the cue onset for marmoset F, and 500 ms before the onset for marmoset E, the reward reaching time changed according to the direction of the induced movement. The difference in the effect of the time window between marmosets E and F might be due to the difference in the extent of the photoactivation and/or stimulation position (39). These results suggest that the voluntary movement was biased toward the movement dominated by the domain of M1 with high activity.

In marmoset G, the mapped M1 was laterally divided into push-, pull-, and push-dominant domains for the hand movement direction. It is therefore necessary to clarify how voluntary arm

reaching in each direction is related to the combination of the neuronal activity in the relevant domain with that in other domains, and 2-photon calcium imaging is useful for this purpose. We previously demonstrated that 2-photon calcium imaging can detect motor cortical activity at a single-cell resolution while a head-fixed marmoset performs a pole-pull/push task and a pole-pull task with velocity-dependent perturbation of pole movement (17). In addition, calcium imaging of the motor cortex with miniature microscopy was applied to naturally behaving marmosets (40). In the present study, the forelimb trajectories could be tracked with a deep learning algorithm applied to the CCD camera images, without the use of any markers. Therefore, all-optical interrogation of motor control can be applied to behaving marmosets. Two-photon calcium imaging has also been recently applied to awake macaques (41). If the current photostimulation method is also effective in other monkeys, all-optical interrogation of the motor control system in behaving nonhuman primates could become prevalent.

Materials and Methods

All experiments were approved by the Animal Experimental Committee of the University of Tokyo. Four laboratory-bred common marmosets were used in the present study. All surgical procedures and AAV injections were performed under aseptic conditions, as described previously (17). All experimental schedules are summarized in *SI Appendix*, Figs. S2 and S8*B*. For ICMS in marmosets E and F, an 11-mm-diameter circular craniotomy with a center at 9.5 mm to 9.75 mm anterior from the interaural line and 4.5 mm to 5.0 mm lateral from the midline was performed, and the dura matter was removed; this site was presumed to be located above M1 (42, 43). In marmoset G, a rectangular craniotomy was performed over the putative M1 and PM (+4.5 mm to 16.5 mm anterior from interaural line, +1.0 mm to +9.0 mm lateral from midline; refs. 42 and 43), and the dura matter was removed. A tungsten microelectrode with an impedance of 0.5 MΩ was inserted to a depth of 1.8 mm from the cortical surface, and a train of 15 cathodal pulses (0.2-ms duration at 200 Hz) were applied. Two CCD cameras equipped with fixed-focus lenses (focal length, 3.0 mm) were orthogonally set 190 mm to the left side and 175 mm in front of the marmoset. The marmosets' hand positions were predicted with DeepLabCut (21). EMG was recorded with a pair of surface silver electrodes with a diameter of 1 mm and a separation of 2 mm. For immunohistochemistry, mouse anti-parvalbumin antibody, Alexa 594 conjugated anti-mouse IgG, and propidium iodide were used. Immuno-in situ hybridization was performed as described previously (44). Data are presented as mean ± SEM, unless otherwise noted. Detailed methods are described in *SI Appendix*. The data supporting the findings of this study are available from the corresponding author upon reasonable request. The data for the photostimulation-induced movements used in Figs. 1–4 have been deposited in figshare (45).

ACKNOWLEDGMENTS. We thank Y. Hirayama and Y. Takahashi for animal handling. We thank R. Hira for preliminary experiments, Y. Isomura for helping to develop the head plate, and Y. R. Tanaka for advice regarding DeepLabCut. We thank K. Deisseroth for providing pAAV-Ef1a-DIO hChR2 (E123T/T159C)-EYFP (Addgene plasmid 35509). This work was supported by Grants-in-Aid for Scientific Research on Innovative Areas (KAKENHI 17H06309 to M.M., KAKENHI 15H05873 to A.N., KAKENHI 18H05059 to Y.M., and KAKENHI 19H05307 to T.E.), for Scientific Research (A) (KAKENHI 15H02350 and 19H01037 to M.M.), for Young Scientists (A) (KAKENHI 17H04982 to Y.M.), for Young Scientists (B) (KAKENHI 17K13277 to T.E.), and for Challenging Research (Exploratory) (KAKENHI 18K19371 to Y.M.) from the Ministry of Education, Culture, Sports, Science, and Technology, Japan; Japan Agency for Medical Research and Development (Grants JP17dm0207050 and JP16dm0207046 to A.N., Grant JP17dm0207001 to T.Y., Grants JP17dm0107053, JP18dm0207027, and JP18dm0107150 to M.M., and Grant JP19dm0207085h0001 to T.E.); Japan Science and Technology Agency, Precursory Research for Embryonic Science and Technology (Grant JPMJPR188B to Y.M.); the Brain Science Foundation (to Y.M.); and the Tokyo Society of Medical Sciences (to T.E.).

1. J. Cavanaugh *et al*., Optogenetic inactivation modifies monkey visuomotor behavior. *Neuron* **76**, 901–907 (2012).
2. I. Diester *et al*., An optogenetic toolbox designed for primates. *Nat. Neurosci.* **14**, 387–397 (2011).
3. A. Galvan *et al*., Nonhuman primate optogenetics: Recent advances and future directions. *J. Neurosci.* **37**, 10894–10903 (2017).
4. X. Han *et al*., Millisecond-timescale optical control of neural dynamics in the nonhuman primate brain. *Neuron* **62**, 191–198 (2009).
5. C. Klein *et al*., Cell-targeted optogenetics and electrical microstimulation reveal the primate koniocellular projection to supra-granular visual cortex. *Neuron* **90**, 143–151 (2016).
6. W. R. Stauffer *et al*., Dopamine neuron-specific optogenetic stimulation in rhesus macaques. *Cell* **166**, 1564–1571.e6 (2016).
7. J. Dai, D. I. Brooks, D. L. Sheinberg, Optogenetic and electrical microstimulation systematically bias visuospatial choice in primates. *Curr. Biol.* **24**, 63–69 (2014).
8. A. Gerits *et al*., Optogenetically induced behavioral and functional network changes in primates. *Curr. Biol.* **22**, 1722–1726 (2012).
9. K. I. Inoue, M. Takada, M. Matsumoto, Neuronal and behavioural modulations by pathway-selective optogenetic stimulation of the primate oculomotor system. *Nat. Commun.* **6**, 8378 (2015).
10. M. Jazayeri, Z. Lindbloom-Brown, G. D. Horwitz, Saccadic eye movements evoked by optogenetic activation of primate V1. *Nat. Neurosci.* **15**, 1368–1370 (2012).
11. S. Ohayon, P. Grimaldi, N. Schweers, D. Y. Tsao, Saccade modulation by optical and electrical stimulation in the macaque frontal eye field. *J. Neurosci.* **33**, 16684–16697 (2013).
12. Y. Lu *et al*., Optogenetically induced spatiotemporal gamma oscillations and neuronal spiking activity in primate motor cortex. *J. Neurophysiol.* **113**, 3574–3587 (2015).
13. T. C. Harrison, O. G. Ayling, T. H. Murphy, Distinct cortical circuit mechanisms for complex forelimb movement and motor map topography. *Neuron* **74**, 397–409 (2012).
14. R. Hira, S. Terada, M. Kondo, M. Matsuzaki, Distinct functional modules for discrete and rhythmic forelimb movements in the mouse motor cortex. *J. Neurosci.* **35**, 13311–13322 (2015).
15. A. Gerits, W. Vanduffel, Optogenetics in primates: A shining future? *Trends Genet.* **29**, 403–411 (2013).
16. D. O'Shea *et al*., Pushing in the wrong direction: Optogenetic perturbation misaligns with motor cortical dynamics. *Front Neurosci.* (Conference Abstract: Computational and Systems Neuroscience [COSYNE], Salt Lake City, UT, 2014).
17. T. Ebina *et al*., Two-photon imaging of neuronal activity in motor cortex of marmosets during upper-limb movement tasks. *Nat. Commun.* **9**, 1879 (2018).
18. O. Sadakane *et al*., Long-term two-photon calcium imaging of neuronal populations with subcellular resolution in adult non-human primates. *Cell Rep.* **13**, 1989–1999 (2015).
19. A. Berndt *et al*., High-efficiency channelrhodopsins for fast neuronal stimulation at low light levels. *Proc. Natl. Acad. Sci. U.S.A.* **108**, 7595–7600 (2011).
20. A. J. Lam *et al*., Improving FRET dynamic range with bright green and red fluorescent proteins. *Nat. Methods* **9**, 1005–1012 (2012).
21. A. Mathis *et al*., DeepLabCut: Markerless pose estimation of user-defined body parts with deep learning. *Nat. Neurosci.* **21**, 1281–1289 (2018).
22. M. S. Graziano, T. N. Aflalo, D. F. Cooke, Arm movements evoked by electrical stimulation in the motor cortex of monkeys. *J. Neurophysiol.* **94**, 4209–4223 (2005).
23. N. Dancause *et al*., An additional motor-related field in the lateral frontal cortex of squirrel monkeys. *Cereb. Cortex* **18**, 2719–2728 (2008).
24. M. S. Graziano, C. S. Taylor, T. Moore, Complex movements evoked by microstimulation of precentral cortex. *Neuron* **34**, 841–851 (2002).
25. S. Schaal, D. Sternad, R. Osu, M. Kawato, Rhythmic arm movement is not discrete. *Nat. Neurosci.* **7**, 1136–1143 (2004).
26. K. J. Burman, S. M. Palmer, M. Gamberini, M. W. Spitzer, M. G. Rosa, Anatomical and physiological definition of the motor cortex of the marmoset monkey. *J. Comp. Neurol.* **506**, 860–876 (2008).
27. M. Wakabayashi *et al*., Development of stereotaxic recording system for awake marmosets (*Callithrix jacchus*). *Neurosci. Res.* **135**, 37–45 (2018).
28. H. Hioki *et al*., High-level transgene expression in neurons by lentivirus with Tet-Off system. *Neurosci. Res.* **63**, 149–154 (2009).
29. N. A. Young, C. E. Collins, J. H. Kaas, Cell and neuron densities in the primary motor cortex of primates. *Front. Neural Circuits* **7**, 30 (2013).
30. T. Kondo *et al*., Histological and electrophysiological analysis of the corticospinal pathway to forelimb motoneurons in common marmosets. *Neurosci. Res.* **98**, 35–44 (2015).
31. K. Nakajima, M. A. Maier, P. A. Kirkwood, R. N. Lemon, Striking differences in transmission of corticospinal excitation to upper limb motoneurons in two primate species. *J. Neurophysiol.* **84**, 698–709 (2000).
32. Z. Gu *et al*., Control of species-dependent cortico-motoneuronal connections underlying manual dexterity. *Science* **357**, 400–404 (2017).
33. R. Hira *et al*., Transcranial optogenetic stimulation for functional mapping of the motor cortex. *J. Neurosci. Methods* **179**, 258–263 (2009).
34. H. Okano *et al*., Brain/MINDS: A Japanese national brain project for marmoset neuroscience. *Neuron* **92**, 582–590 (2016).
35. A. Iwanami *et al*., Establishment of graded spinal cord injury model in a nonhuman primate: The common marmoset. *J. Neurosci. Res.* **80**, 172–181 (2005).
36. K. Sato *et al*., Generation of a nonhuman primate model of severe combined immunodeficiency using highly efficient genome editing. *Cell Stem Cell* **19**, 127–138 (2016).
37. I. Tomioka *et al*., Transgenic monkey model of the polyglutamine diseases recapitulating progressive neurological symptoms. *eNeuro* **4**, ENEURO.0250-16.2017 (2017).
38. O. A. Gharbawie, I. Stepniewska, J. H. Kaas, Cortical connections of functional zones in posterior parietal cortex and frontal cortex motor regions in new world monkeys. *Cereb. Cortex* **21**, 1981–2002 (2011).

39. M. M. Churchland, K. V. Shenoy, Delay of movement caused by disruption of cortical preparatory activity. *J. Neurophysiol.* **97**, 348–359 (2007).
40. T. Kondo *et al*., Calcium transient dynamics of neural ensembles in the primary motor cortex of naturally behaving monkeys. *Cell Rep.* **24**, 2191–2195.e4 (2018).
41. M. Li, F. Liu, H. Jiang, T. S. Lee, S. Tang, Long-term two-photon imaging in awake macaque monkey. *Neuron* **93**, 1049–1057.e3 (2017).
42. C. D. Hardman, K. W. S. Ashwell, *Stereotaxic and Chemoarchitectural Atlas of the Brain of the Common Marmoset (Callithrix jacchus)* (CRC Press, Boca Raton, FL, 2012).
43. S. Yuasa, K. Nakamura, S. Kohsaka, *Stereotaxic Atlas of the Marmoset Brain* (Igaku Shoin, Tokyo, Japan, 2010).
44. A. Watakabe, Y. Komatsu, S. Ohsawa, T. Yamamori, Fluorescent in situ hybridization technique for cell type identification and characterization in the central nervous system. *Methods* **52**, 367–374 (2010).
45. T. Ebina, M. Matsuzaki, Arm movements induced by non-invasive optogenetic stimulation of the motor cortex in the common marmoset. FigShare. https://dx.doi.org/10.6084/m9.figshare.9918887. Deposited September 30 2019.